

## Regular Article

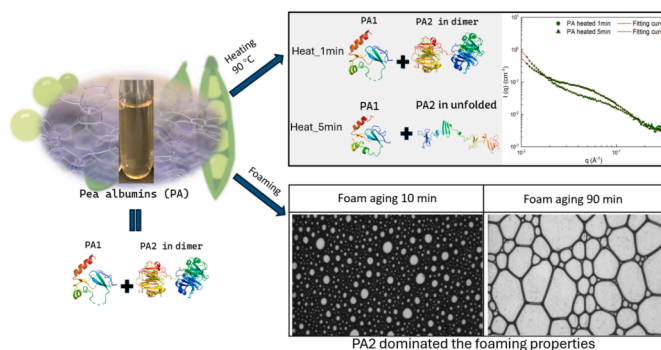
## In-depth exploration of the structure of pea albumin, its fractions and their heating and foaming properties

Ruifen Li<sup>a,\*</sup>, Dionysios Neofytos<sup>a</sup>, Jacob J.K. Kirkensgaard<sup>b,c</sup>, Antara Pal<sup>d</sup>, Jan Skov Pedersen<sup>d,\*\*</sup>, Milena Corredig<sup>a,e,\*</sup><sup>a</sup> Food Science Department, Aarhus University, Aarhus 8200, Denmark<sup>b</sup> Department of Food Science, University of Copenhagen, Rolighedsvej 26, DK-1958 Frederiksberg C, Denmark<sup>c</sup> Niels Bohr Institute, Universitetsparken 5, 2100 København Ø, Denmark<sup>d</sup> Department of Chemistry and Interdisciplinary Nanoscience Center, Aarhus University, 8000 Aarhus, Denmark<sup>e</sup> Department of Process and Life Science Engineering, Lund University, 22100, Sweden

## HIGHLIGHTS

- Pea albumins contain various isoforms of PA1 and PA2;
- PA1 and PA2 SAXS data can be modeled at high-resolution models based on AlphaFold predictions;
- PA1 is present as a monomer, PA2 is predominantly a dimer at pH 7;
- Pea albumins heat-induced aggregation can be modeled as a combination of PA1 and PA2;
- Foaming properties of pea albumins can be attributed predominantly to PA2.

## GRAPHICAL ABSTRACT



## ARTICLE INFO

## Keywords:

Pea albumins  
PA1  
PA2  
Secondary structure  
SAXS  
Interfacial properties  
Foaming  
Heat-induced aggregates

## ABSTRACT

**Hypothesis:** The structure and functionality of pea albumin can be described in detail as a combination of its main fractions, PA1 and PA2.

**Experimental:** PA1 and PA2 were purified from a Pea Albumin extract (PA) using size exclusion chromatography, and characterized by two-dimensional gel electrophoresis. Their secondary structure was analyzed using Fourier-Transform Infrared Spectroscopy (FTIR). The structures before and after heat treatment (90 °C, 1 & 5 min) were investigated by Small-Angle X-ray Scattering (SAXS). SAXS intensities were evaluated using high-resolution models obtained as predictions from the AlphaFold Protein Structure Database. Interfacial and foaming properties were also evaluated.

**Findings:** Both PA1 and PA2 contained various isoforms, and PA2 displayed a high  $\beta$ -sheet/ $\alpha$ -helix ratio. In solution, SAXS intensities of PA1 could be predicted by its native structure, and after heating PA1 showed limited aggregation. PA2 could be presented as a dimer, which unfolded and formed large aggregates during heating. The high-resolution models could also explain well the SAXS signal of the unfractionated PA, combining PA1 and

\* Corresponding authors at: Food Science Department, Aarhus University, Aarhus 8200, Denmark.

\*\* Corresponding author at: Department of Chemistry and Interdisciplinary Nanoscience Center, Aarhus University, 8000 Aarhus, Denmark.

E-mail addresses: [ruifen@food.au.dk](mailto:ruifen@food.au.dk) (R. Li), [jsp@chem.au.dk](mailto:jsp@chem.au.dk) (J.S. Pedersen), [mc@food.au.dk](mailto:mc@food.au.dk) (M. Corredig).

<https://doi.org/10.1016/j.jcis.2025.137507>

Received 22 February 2025; Received in revised form 1 April 2025; Accepted 2 April 2025

Available online 3 April 2025

0021-9797/© 2025 The Author(s). Published by Elsevier Inc. This is an open access article under the CC BY license (<http://creativecommons.org/licenses/by/4.0/>).

PA2. After heating, PA2 dominated the properties of the PA mixtures. PA2 predominantly contributed to the interfacial and foaming properties of PA, in spite of both PA1 and PA2 showing adsorption at the air/water interface. Indeed, PA1 in isolation could not form a stable foam.

*Perspective:* SAXS data analyzed with high-resolution structure models allowed for an in depth understanding of the structural changes of PA1 and PA2, and provided a mechanistic understanding of the relationships between structure, composition, and technological functionality of the albumin fractions from pea.

## 1. Introduction

In recent years, the dietary shift from animal- to plant-based protein sources for food has gained significant attention due to growing concerns over sustainability, environmental impact, and the need for diversified food resources. Thus, exploring alternative protein sources is of great importance, leading to an increased need to understand how the proteins can be used as ingredients in foods. Among the legume proteins, pea proteins have emerged as a promising candidate. Albumins, accounting for 8–20 % of the total protein from pea [1], are water/acid-soluble proteins commonly recovered as a side stream during acid precipitation of their counterparts, globulins [2]. Recently, it has been suggested that plant-derived albumins may show better technological functionality than the globulins, due to their solubility in a wide range of pH and their emulsifying and foaming properties [3–8]. However, most of the studies have so far been limited to the entire albumin extract, posing challenges in deriving a mechanistic understanding of the structure–function relationships of the protein present in the mix.

Pea albumins comprise two main protein fractions, PA1 and PA2. These proteins account for 50 % and 16 % of the seed's total sulfur-containing amino acids, respectively [9]. The amino acid sequence of these two fractions have been determined earlier in [10] and [11], with their high-resolution structure predictions published in the AlphaFold Protein Structure Database under entries P62927 and P08688, respectively [12]. The pre-protein of PA1 molecule contains 130 amino acids, while the PA2 molecule is composed of 230 amino acids, containing four imperfect repeat sequences, each approximately 57 amino acids in length. PA1 constitutes approximately 7 % of the total pea seed protein, and after cleaving off the signal peptide, its structure is composed of two subunits when *endo*-proteolytically cleaved, resulting in a PA1a (molecular weight, MW 6 kDa, residues 70–122) and PA1b (MW 4 kDa, residues 28–62) fraction. In contrast to many other plant albumins, PA1 subunits are not connected by an interchain disulfide bond [13]. Its structure is defined by a triple-stranded antiparallel  $\beta$ -sheet with a long flexible loop [14]. PA2 is larger than PA1, it has a MW of 26 kDa. PA2 plays a crucial role in enhancing the nutritional value of pea seeds [11], and it is present in two forms PA2a and PA2b [15], non-covalently associated, forming homodimers of 53 and 48 kDa, respectively [16]. Unlike all the other major pea seed proteins, PA2 is found in the cytosol instead of within protein bodies [16], lacks glycosylation, is synthesized without a signal sequence, and undergoes minimal post-translational processing [11].

To fully exploit the potential of PA as an ingredient, it is essential to gain a fundamental understanding of the physicochemical properties of these proteins, to investigate the distinct structure, characteristics, and technological functionalities of the purified PA1 and PA2 fractions from whole pea albumin isolates. Only by carrying out a more in-depth study, will it be possible to uncover their full potential and leverage them in food and colloidal applications.

In this study, the soluble Pea Albumin Fraction (PA) was studied and compared to the two components, PA1 and PA2, purified using size exclusion chromatography. The structure was evaluated using FTIR and Small-Angle X-ray Scattering (SAXS). Heating stability was evaluated by analyzing the protein solutions before and after heating (90 °C for 1 and 5 min). The interfacial and foaming properties were also investigated. This research brings valuable insights into the mechanisms underpinning structure–function relationships of these proteins, in particular

their heating and foaming properties, and will aid in their optimal application as functional ingredients in food products.

## 2. Material and methods

### 2.1. Materials

Pea protein concentrate (0.55 kg protein/kg solids), a product of milling and air classification, was kindly provided by Vestkorn A/S (Holstebro, Denmark). The concentrate also contained lipids and carbohydrates as well.

All the other chemicals, e.g., hydrochloric acid, sodium hydroxide, monosodium phosphate, disodium phosphate, sodium chloride, and sodium azide, used in this study are analytical grades and obtained from Merck (Merck Life Science A/S, Søborg, Denmark).

### 2.2. Sample preparation

A whole albumin isolate (PA) was separated from the other pea proteins (i.e., globulins) using isoelectric precipitation [17]. In brief, after centrifugation of the protein extract at pH 4.5, the supernatant was dialyzed and then freeze-dried into powder, stored at  $-20$  °C until further use [17]. The protein content was analyzed using Pierce BCA protein assay kit (Thermo Scientific, Rockford, U.S.A.), converting to  $\sim 0.70$  kg ( $\pm 0.001$ ) protein per kg of solids in its powder form. The residual fraction was mostly composed of carbohydrates ( $\approx 0.30 \pm 0.002$  kg/kg) and measured using Phenol-Sulfuric Acid Method [18], as the ash content measured was only approximately  $2 \pm 1$  g/kg.

The two main albumin fractions (PA1 and PA2) were isolated from the PA extract using preparative size exclusion chromatography. In brief, PA freeze-dried powder was reconstituted in MiliQ water (30 mg protein/mL) overnight at 4 °C. Then the PA solution was applied onto a Sephacryl S-100 column (HiPrep 16/60, Cytiva, United States) at a flow rate of 0.5 mL/min with peak elution volume of 1 mL. The chromatographic separation was performed using 50 mM sodium phosphate buffer (38 mM  $\text{Na}_2\text{HPO}_4$  and 12 mM  $\text{NaH}_2\text{PO}_4$ ), containing 150 mM NaCl and 0.2 mg/mL sodium azide (pH 7.2). The fractions were then collected according to their separate peaks in the elution profile monitored by UV absorbance at 280 nm. Then their protein molecular weights were analyzed by SDS-PAGE using NuPAGE 12 % Bis-Tris gel (12 well, Invitrogen) with Spectra™ Multicolor Broad Range Protein Ladder (5  $\mu\text{L}$ ) as reference. The gel was stained with Coomassie Brilliant blue staining and imaged on a Gel Doc™ EZ System using Image Lab™ software (BIO-RAD laboratories, USA). Finally, the fractions of PA1 and PA2 were desalted using 3 kDa pre-hydrated dialysis tubes, and freeze-dried into powder, stored at  $-20$  °C until further use.

### 2.3. Two-dimensional (2D) gel electrophoresis

The purified protein fractions were analyzed by 2D gel electrophoresis under reducing conditions for their isoform analysis. In brief, the samples were first diluted in lysis buffer (7 M urea, 2 M thiourea, 1 % DTE (dithioerythritol), 40 mM Tris-Base, pH 7.5) of 200  $\mu\text{L}$ , incubated for 1 h under shaking. Then the protein solution was focused onto 11 cm immobilized pH gradient (IPG) strips (pH 4–7) (BIO-RAD) using active rehydration (500 V, 12 h at 22 °C) in a PROTEAN IEF (isoelectric focusing) Cell (BIO-RAD). The strips were focused at 250 V for 15 min to

8000 V in 2.5 h and maintained until 35,000 V was reached. The gradient gels (BIO-RAD) of 4 – 15 % were then used to perform the electrophoresis according to [19], and Coomassie brilliant blue was used for the staining step.

#### 2.4. Fourier-transform infrared spectroscopy (FTIR)

FTIR analysis was performed using a Perkin Elmer Spectrum 3 Mid-IR Spectrometer equipped with a macro-attenuated total reflection Fourier transform infrared (ATR-FT-IR) unit. The ATR element comprised a thallium bromoiodide (KRS-5)-based diamond with a one-bounce configuration. Before each measurement, background spectra were collected using a clean ATR crystal exposed to air to minimize any environmental contributions in the acquired spectra. Spectra were collected in the mid-infrared region (4000 – 400  $\text{cm}^{-1}$ ) at a spectral resolution of 4  $\text{cm}^{-1}$ . To enhance the signal-to-noise ratio, each measurement comprised 30 co-added scans.

As the presence of water significantly impacts the FTIR signal [20], samples were carefully prepared. The freeze-dried samples, PA, PA1, and PA2 were rehydrated to a final concentration of 2 mg/mL in  $\text{D}_2\text{O}$  to restore their hydrated conformation, allowing the protein molecules to regain their native conformation. After rehydration and prior to data collection, 2  $\mu\text{L}$  of the protein solution was deposited onto the ATR crystal, forming a thin, hydrated film of the sample through partial solvent evaporation [21,22]. No external pressure was applied between the sample and the ATR crystal during measurements, as film formation resulted in perfect contact between the crystal and the protein film.

Before spectral analysis, automatic ATR correction and  $\text{CO}_2/\text{H}_2\text{O}$  subtraction were performed. As FTIR analysis focused on the interpretation of the amide I region (1700 – 1600  $\text{cm}^{-1}$ ), this area was isolated from the rest of the spectrum. A linear baseline correction between the two baseline points was applied, followed by smoothing using a Savitzky-Golay filter with a 5-point window and 1st-order polynomial fitting, and normalization of the amide I band.

A manual supervised analysis of the secondary structure elements of the proteins was conducted by deconvoluting the amide I band into individual subcomponent peaks representing different protein secondary structures. This analysis was performed by applying Gaussian curve fitting to the 'pea lectin I band using Quasar [23,24] and Fityk software [25]. The positions of subcomponent peak centers were determined based on literature values: aromatic rings (1600 – 1615  $\text{cm}^{-1}$ ),  $\beta$ -sheets (1620 – 1640  $\text{cm}^{-1}$  and 1665 – 1680  $\text{cm}^{-1}$ ), random coils (~1630 – 1645  $\text{cm}^{-1}$ ),  $\alpha$ -helices (~1648 – 1660  $\text{cm}^{-1}$ ), turns and bends (~1670 – 1680  $\text{cm}^{-1}$ ), and non-attributed peaks (~1690 1700  $\text{cm}^{-1}$ ) [26,27]. Following deconvolution, the percentage of each secondary structure element was calculated by dividing the area of each peak by the total area of the peaks. Manual analysis was preferred for peak deconvolution, to avoid potential errors occurring when applying automated deconvolution algorithms. A protein's secondary structure elements significantly influence their flexibility, resistance to temperature treatment, as well as their interfacial and functional properties, with  $\alpha$ -helix and  $\beta$ -sheet content playing a critical role in protein emulsifying and foaming behavior [28].

#### 2.5. Small-angle X-ray scattering (SAXS)

The unfractionated mix PA, as well as the single PA1 and PA2 fractions were measured at a constant protein concentration (10 mg/mL) in MilliQ water using SAXS. Samples were measured before and after heating at pH 7. The experiments were conducted using laboratory equipment (Nano-inXider, Xenocs SAS, Grenoble, France), equipped with a  $\text{CuK}\alpha$  source with a 1.54  $\text{\AA}$  wavelength and a resulting  $q$  range of 0.01 to 0.37  $\text{\AA}^{-1}$ .

Borosilicate capillary tubes were used, and samples were degassed for 5 min in a desiccator at room temperature before SAXS measurements. Each sample was then measured at a total acquisition time of 60

min at room temperature. Milli-Q water was used as the background. Data reduction and background subtraction was performed using the XSACT software. The data are presented as intensities  $I(q)$  as a function of  $q$ , the modulus of the scattering vector.

The radius of gyration ( $R_g$ ) at high  $q$  range was determined by both a Guinier fit and Indirect Fourier Transformation (IFT), which are model independent. The SAXS data in this study show a clear Guinier region or 'shoulder' at intermediate  $q$ , thus this method is justified for the cases. The Guinier fit estimated  $R_g$  from the slope fitting  $I(q) = I(0)e^{-q^2R_g^2/3}$  when the SAXS scattering data are linear in the Guinier plot of  $\ln(I(q))$  vs  $q^2$ . IFT provides the pair distance distribution function  $p(r)$  and also  $R_g$ .

The SAXS data was analyzed using high-resolution structures based on the AlphaFold predictions P62927 and P08688, respectively [12]. Calculations of theoretical SAXS curves of the proteins originated from the high-resolution structural data using the method described in detail elsewhere [29,30]. Some of the data sets showed a power law scattering at low  $q$  due to the presence of large aggregates; in this case, a power-law structure factor was included:  $S(q) = 1 + a/q^b$  where  $a$  and  $b$  are fit parameters and the factor is included to obtain better stability of the fits. For the PA2 data, a cluster structure factor was included since the SAXS data show signs of some unspecific aggregation [30]. In case both structure factors were required, the combined structure factor was taken as the product of the two. In the implementation, the decoupling approximation was used as described in [30]. In addition to PA1 and PA2 proteins in isolation, the unfractionated PA samples were also analyzed, and could be reproduced by a linear combination of the scattering from PA1 and PA2 and a power-law scattering. Note that the dimer PA2 model of SAXS data was determined using rigid-body refinement with random searches employing connectivity and excluded volume restraints and imposing C2 ( $P_2$ ) symmetry [30]. Also, the unfolded structure of PA2 at high temperature was obtained by rigid-body refinement dividing the predicted structure into smaller bodies.

#### 2.6. Interfacial properties

The Interfacial adsorption behaviors and dilatational rheology of samples at the air–water interfaces were measured using a pendant drop tensiometer (Surface Analyzer LSA100, LAUDA Scientific GmbH, Germany). A drop (25  $\text{mm}^2$ ) of protein solution at 0.1 % (w/w) was firstly generated in the air at the tip of a needle, and then followed by monitoring of the real-time interfacial tension for approximately 3 h. During this measurement, the drop was protected in a sealed cuvette which could also prevent evaporation. The Young-Laplace equation was used to estimate interfacial tension by fitting the drop contour for pendant drop analysis. Subsequently, the same drop was performed sinusoidal oscillatory deformations using amplitude sweeps starting from 3 % to 30 % at a fixed frequency of 0.02 Hz. Each amplitude was run for five cycles. The amplitude sweeps results were then fitted the surface dilatational elastic modulus ( $E_d'$ ) as a function of frequency ( $\omega$ , Hz). These experiments were performed at least in triplicate at room temperature of 22  $^\circ\text{C}$  ( $\pm 1^\circ\text{C}$ ).

#### 2.7. Foam properties

The properties of foams were studied using the FOAMSCAN apparatus (Teclis, Lyon, France) by injecting 60 mL of the foaming solution into the column. Then, air flowed at 50 mL/min through the porous frit (16  $\mu\text{m}$  in diameter) under the solution and stopped when the foam volume reached 250 mL. Afterwards, the foam was monitored under free drainage conditions for 90 min with the volume of its foam, liquid drainage and bubbles images recorded. Measurements were done in triplicates from a fresh foaming solution each time.

## 2.8. Statistical analysis

SPSS Statistics 28 (IBM, New York, USA) was used for statistical analysis. ANOVA (one-way analysis of variance) was carried out following Tukey's multiple comparison test based on a statistical significance level of  $P < 0.05$ .

## 3. Results and discussion

### 3.1. Protein purification and polypeptide composition

The elution profile of the PA fraction, as monitored by UV absorbance at 280 nm, is displayed in Fig. 1. Three main fractions were collected and analyzed by SDS-PAGE, to determine their composition. As marked in Fig. 1, PA2 eluted mainly in the peak around 50 mL, while PA1 was more widely distributed, in both the peak at 60 mL and eluting later, between 70 and 80 mL. The PA1 collected for analysis was the latter. PA1 displayed a band around 10 kDa, while PA2 displayed a sharp band at 25 kDa, in agreement with previous studies [7,8]. Note that the 10 kDa band for PA1 would suggest binding of more than one protein per SDS micelle. Due to the lack of purity, the middle peak was not further analyzed. The AlphaFold [12] structures for PA1 and PA2 are also displayed in Fig. 1, and are based on P62927 and P08688, respectively.

The composition of PA and the corresponding PA1 and PA2 isolated fractions was further characterized by 2D gel electrophoresis. PA showed three main protein bands (bands 1, 2, and 3), corresponding to approximately 10, 18, and 25 kDa, respectively. The 2D gel revealed nine major protein spots (Fig. 2). The PA1 and PA2 fractions clearly showed the presence of spots 1, 2, and 3 and spots 7, 8, 9 respectively. PA2 also showed an additional faint spot (spot 5). The presence of separated spots in PA1 and PA2 fractions clearly indicated the presence of isomers within them. The results are in contrast to previous findings

who identified five well-separated spots for PA1 [31,32]. The two spots in Fig. 2 marked 4 and 5 in PA (~18 kDa), have been previously reported to match chain A, pea lectin alpha chain [28]. In the case of PA2, the absence of spots 4 and 6, when compared to PA, suggests their elution in the middle peak during the size exclusion purification process (Fig. 1).

### 3.2. Secondary structure of pea albumin fractions

Pea albumins were studied using FTIR to investigate their secondary structures. Fig. 3 presents the results for the amide I band peak deconvolution, including the fitted underlying subcomponent peaks and the resulting convoluted peak obtained by peak reconstruction.

The estimated secondary structure elements for each protein are described in Table 1. The secondary structure content (PA1 and PA2) determined by FTIR agrees with the predicted protein structure from AlphaFold, as well as prior literature, describing proteins with very low helical structure [11,14]. Both PA1 and PA2 contained  $\beta$ -sheet and  $\alpha$ -helical structural elements. All samples exhibited a low proportion of  $\alpha$ -helix, below 20 % of the total signal. FTIR analysis also revealed significant differences in the other major structural features: PA1 presented the lowest  $\beta$ -sheet content (~15 %) and the highest random coil content (33 %), while PA2 exhibited the highest  $\beta$ -sheet content (27 %) and the lowest helical content (9 %). The PA fraction, as expected, composed of both protein fractions, provided intermediate secondary structure values.

Previous work has suggested that a higher  $\beta$ -sheet content might result in low surface activity [8,33]. However, a higher proportion of random coils may result in a more adaptable protein structure, capable of undergoing conformational changes. In the context of interfacial adsorption, i.e. during foam formation, this adaptability may facilitate the rearrangement of protein molecules at the air-water interface. A more flexible protein structure can readily adapt to the dynamic

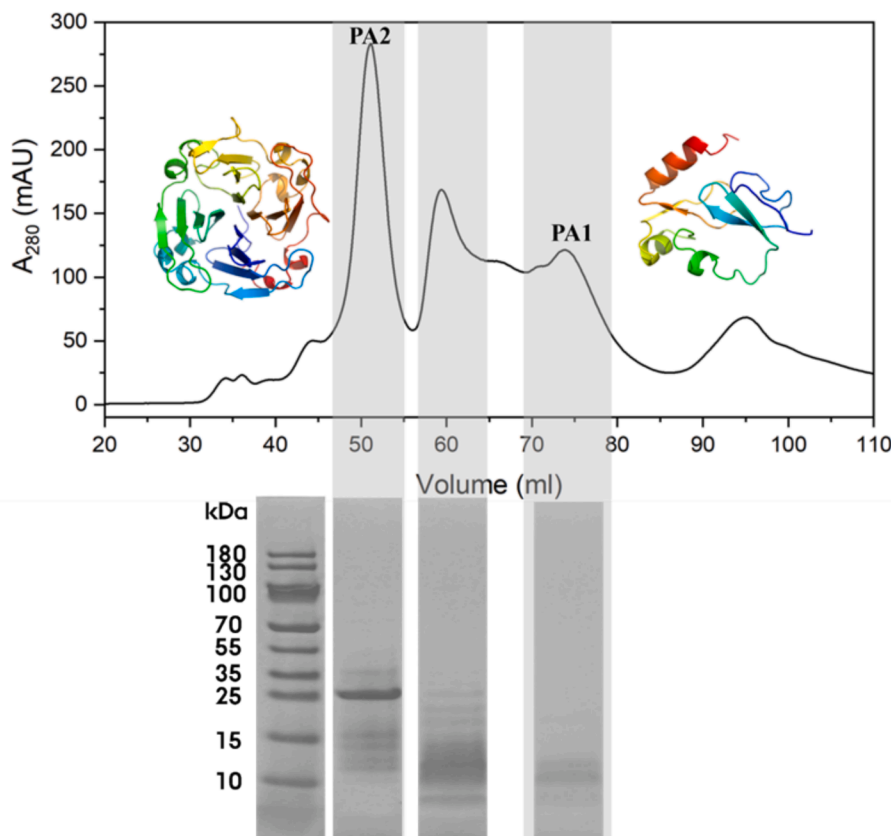
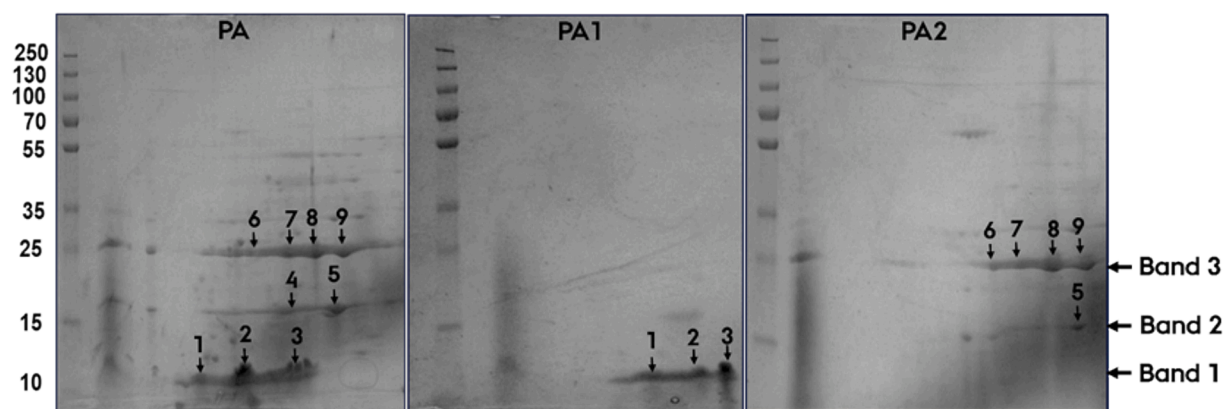
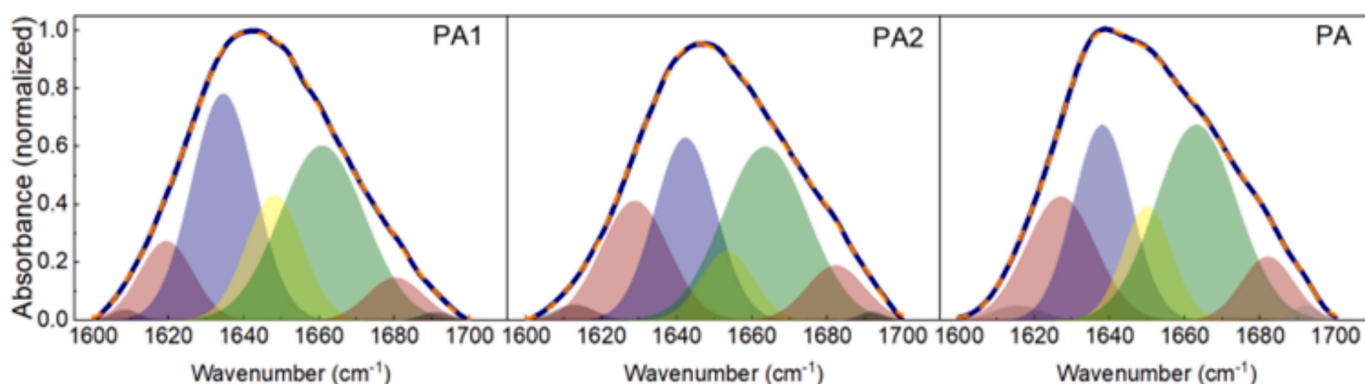


Fig. 1. Elution profile of pea albumins solution using size exclusion chromatography with Sephacryl S-100 column, with collected peaks identified, together with their corresponding SDS-PAGE profile. MAU represent milli-absorbance unit.



**Fig. 2.** Two-dimensional gel electrophoresis of PA and its fractions (PA1 and PA2), extracted by size exclusion chromatography. Bands were stained using Coomassie brilliant blue. (For interpretation of the references to colour in this figure legend, the reader is referred to the web version of this article.)



**Fig. 3.** Amide I band deconvolution of PA1, PA2 and PA pea albumin fractions from left to right. The Amide I band is shown as a solid blue line, and the fitted peak after convolution of the deconvoluted peaks is shown as an orange dashed line. Deconvoluted peaks representing each of the secondary structure elements are shown from left to right: aromatic rings,  $\beta$ -sheets, random coils,  $\alpha$ -helices,  $\beta$ -sheets, turns and bends, non-attributed peaks. Measurements were in triplicate. (For interpretation of the references to colour in this figure legend, the reader is referred to the web version of this article.)

**Table 1**

Secondary structure elements estimates for the three samples (PA1, PA2, and PA). The table presents the ratio (percentage) of aromatic rings,  $\alpha$ -helix,  $\beta$ -sheet, random coil, turns and bends for each sample, as determined by Amide I analysis. Measurements were in triplicate.

	PA1	PA2	PA
Aromatic Rings	$0.7 \pm 0.04$	$1.6 \pm 0.10$	$1.6 \pm 0.10$
$\beta$ -sheets	$15.3 \pm 0.92$	$27.0 \pm 1.62$	$26.1 \pm 1.57$
Random Coils	$33.1 \pm 1.99$	$26.8 \pm 1.61$	$24.8 \pm 1.49$
$\alpha$ -Helixes	$16.3 \pm 0.98$	$8.7 \pm 0.52$	$12.2 \pm 0.73$
Turns & Bends	$34.1 \pm 2.05$	$35.4 \pm 2.12$	$34.7 \pm 2.08$
Non-attributed peaks	$0.6 \pm 0.04$	$0.5 \pm 0.03$	$0.5 \pm 0.03$

interfacial environment, effectively spreading and forming a cohesive protein film. Compared to other well-known foaming proteins, such as ovalbumin [35] and  $\beta$ -lactoglobulin [36], pea albumins show a lower ratio of  $\beta$ -sheet (15–27 % to 38–50 %) and higher ratio of random coil contents (25–33 % to 12–20 %). Additionally, the tertiary structure modification and orientation of the hydrophobic domains are known to play a key role during protein adsorption at the interface [34]. For example, previous literature has indicated that PA2 exhibits high conformational adaptability at oil–water interface, but predominantly due to the presence of aggregates composed of rigid globular structures interconnected by intermolecular disulfide bonds [37].

### 3.3. Structure of pea albumins and their heat-induced changes

PA1, PA2 and PA solutions were subjected to heating at 90 °C for 1 and 5 min. The visual appearance of the samples before and after heating is presented in Fig. 4. The PA1 solutions remained clear throughout the heating process. However, both the PA2 and whole albumins PA became turbid after 1 min of heating. The aggregates formed in the PA2 solution appeared to remain dispersed in solution after heating; however, in the case of the whole, unfractionated PA sample, a clear two-phase system was formed, which could be easily separated by low-speed centrifugation. These findings were consistent with the presence of extensive protein aggregation.

To better understand the structural changes at multiple length scales in the various protein samples, the solutions were subjected to SAXS analysis. The scattering data and the model curves of the samples are shown in Fig. 5, together with the determined structures. In the case of PA1 unheated solutions, the scattering curves were analyzed using the PA1 structure from AlphaFold (P62927) [12]. For the heat-treated PA1 solutions, both 1 and 5 min, a power-law factor was also introduced to analyze the upturn observed in the low- $q$  range, signaling the formation of heat-induced aggregates. This upturn in the scattering signal at low  $q$  vectors ( $\leq 0.03 \text{ \AA}^{-1}$ ) showed a power-law factor of  $q^{-2.2}$  and  $q^{-3.1}$  at 1 and 5 min, respectively (Fig. 5A). Despite the upturn at low  $q$ , the local structure in the high  $q$  range ( $> 0.03 \text{ \AA}^{-1}$ ) was unchanged, indicating that the proteins were still folded after heating (Fig. 5A). It is important to note that these solutions were clear after heating (Fig. 4), hence, these aggregates, within the current experimental conditions, were soluble. By analyzing the data, omitting the low- $q$  part with the power-law

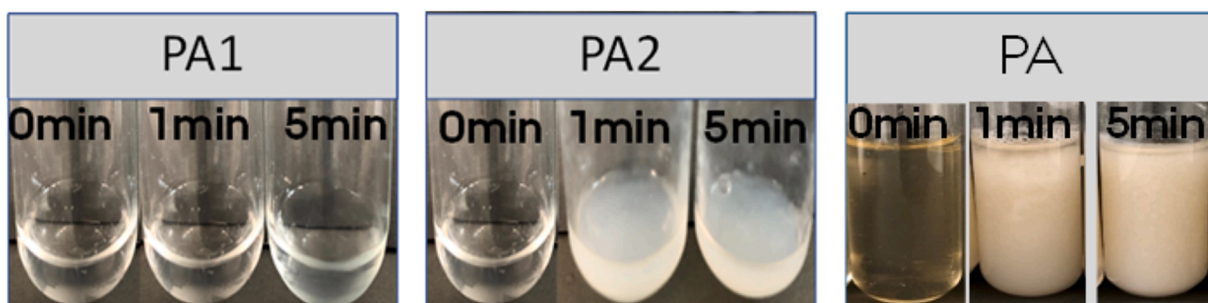


Fig. 4. Visual observations of pea albumin fractions solutions (10 mg/ml) after heat treatment at 90°C for 0, 1, and 5 min.

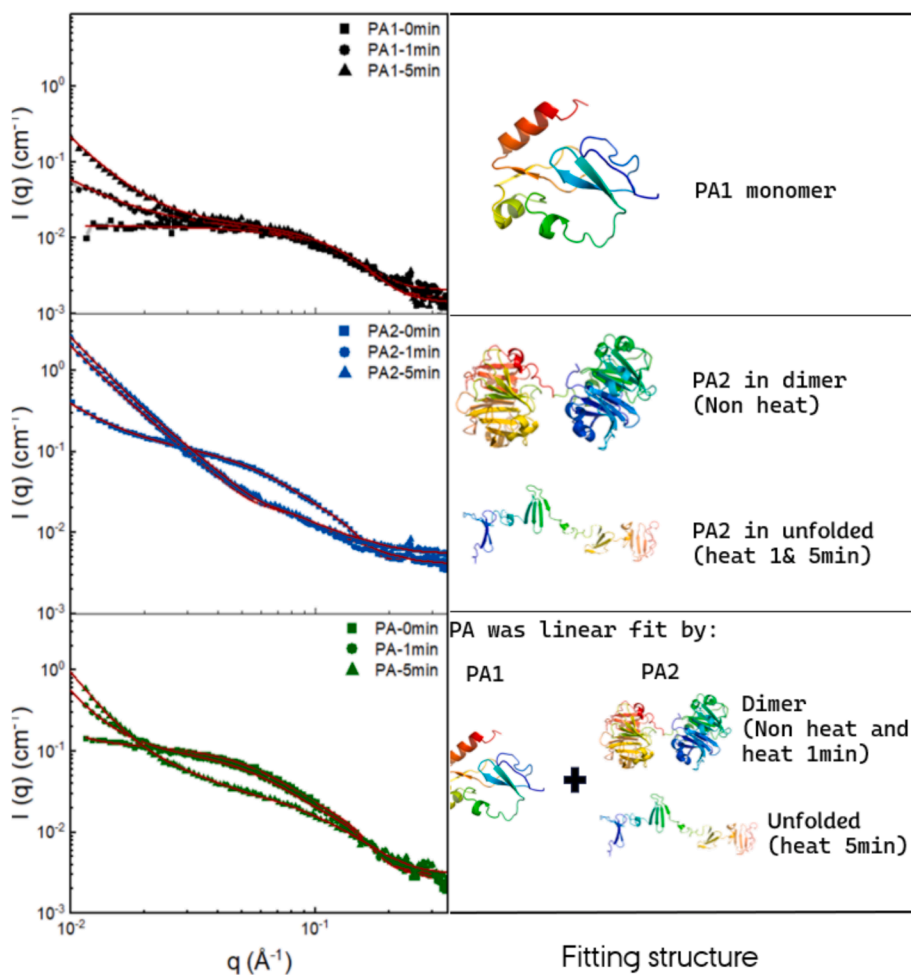


Fig. 5. Background-subtracted X-ray scattering intensity as a function of  $q$  for 10 mg/mL solutions of pea albumins, PA1, PA2, and the unfractionated PA, before (filled squares) or after heating at 90 °C for 1 (filled circles) and 5 min (filled triangles). Red lines represent their model fits based on high-resolution models from AlphaFold structures or PyMol fragmentation. (For interpretation of the references to colour in this figure legend, the reader is referred to the web version of this article.)

scattering for the heat-treated samples with both Guinier and IFT (only low  $q$  before upturn), gave estimates for  $R_g$  for PA1 of around 14–17 Å, (Table 2, Fig. 6). The  $p(r)$  function is essentially unchanged when heating the samples with a maximum diameter of 45 Å.

For PA2 solutions, the initial, unheated protein SAXS intensities were fitted using a high-resolution model using the structure predicted from AlphaFold (P08688) [12]. A dimer assembly was used for the unheated PA2 solution at pH 7, as established in the literature. The dimer PA2 model of SAXS data was determined using rigid-body refinement imposing C2 (P2) symmetry [30]. The estimated radius ( $R_g$ ) when omitting the lowest  $q$  range with the power-law scattering both Guinier

and IFT fits was 22–24 Å (Table 2), with  $p(r)$  functions with a maximum diameter of 85–90 Å (Fig. 6). After heating for 1 and 5 min, the X-ray scattering intensity at high  $q$  was significantly lower than for the unheated samples, indicating a substantial decrease in the population of the constituting units of PA2, responsible for the form factor at this  $q$  range. To model the SAXS data for the PA2 heated solutions, the initial PA2 structure derived from AlphaFold was divided using PyMOL [38] (Molecular Graphics System, Version 1.8.) into 11 bodies consisting of well-defined structural elements of  $\beta$ -sheets and  $\alpha$ -helical structures. Furthermore, rigid-body optimization was performed as described in [30], employing random searches with connectivity and excluded

**Table 2**

Summary of fitting parameters and models employed to evaluate SAXS scattering profiles for pea albumins solutions (10 mg/mL), namely, PA1, PA2, and PA before or after heating at 90 °C for 1 and 5 min.

heating time (min)	Model employed	$R_g$ (Å) from Guinier fit	$R_g$ (Å) from IFT	Power exponent	
	High- $q$ range	Low $q$ -range	$q$ range without power-law scattering	Low- $q$ range	
PA1 0	Monomer structure	Power law	14	14	
1			16	17	2.2
5			17	17	3.1
PA2 0	Dimer structure	Power law	25	24	2.5
1			Unfolded structure		3
5			Unfolded structure		3.1
PA 0	Linear combination of PA1 and PA2 (PA2 in dimer for 0& 1 min, unfolded for 5 min)		24	23	3.4
1			24	22	3.7
5					3.8

volume restraints. As in PA2, all the SAXS data displayed an upturn at low  $q$ . Consequently, a power law structure factor was used to analyze all the samples, revealing the dependencies of  $q^{-2.5}$  for unheated solution, and  $q^{-3}$  and  $q^{-3.1}$ , for solutions with increasing heating times (Table 2). This upturn indicated the formation of protein aggregates. For PA2, these aggregates caused the heated solution to appear visually

turbid, as shown in Fig. 4.

Fig. 5 also shows the X-ray scattering intensity for the unfractionated PA, before and after heating. In this case also, there was a clear structural feature at high  $q$  and an increase in intensity at low  $q$  upon heating. The SAXS data for unheated PA solutions was reproduced by a linear combination of the high-resolution models corresponding to PA1 and the PA2 dimer. The ratio between the two proteins (corresponding to relative concentration) was  $\sim 2$ , a value lower than the  $\sim 3.1$  ratio reported previously [7]. The  $R_g$  values calculated from Guinier plots, as well as  $p(r)$  functions, were similar to those measured for PA2, with  $R_g$  of about 23 Å. This suggests that the scattering signal is dominated by PA2, as expected, due to the higher MW of the PA2 dimer compared to the PA1 monomer. PA solutions heated for 1 min at 90 °C showed an obvious upturn at low  $q$ , but with the local structure at high  $q$  nearly unaltered. After 1 min heating, the same model used for the unheated solution fit the SAXS data, in contrast with what was observed for the PA2 in isolation, which showed extensive unfolding already after 1 min. This discrepancy would indicate that after 1 min of heating in the unfractionated PA, both the presence of PA1 and other contaminants, such as soluble polysaccharide, may protect PA2 from unfolding. These results confirm our previous work using size exclusion chromatography coupled with multi-angle laser light scattering (SEC-MALS) [17], which suggested the stability of PA1 in a PA mixture. The PA solution, after heating for 5 min showed a significant decrease in X-ray scattering intensity at intermediate to high  $q$ , similar to what has been observed for pure PA2. In this case, it was possible to reproduce the SAXS data using a linear combination of the scattering for the native PA1 and unfolded PA2 (Fig. 5, Table 2), suggesting that the residual scattering feature at high  $q$  may be related to PA1. The upturn at low  $q$  in the PA samples showed an increase in exponent with heating time, suggesting the

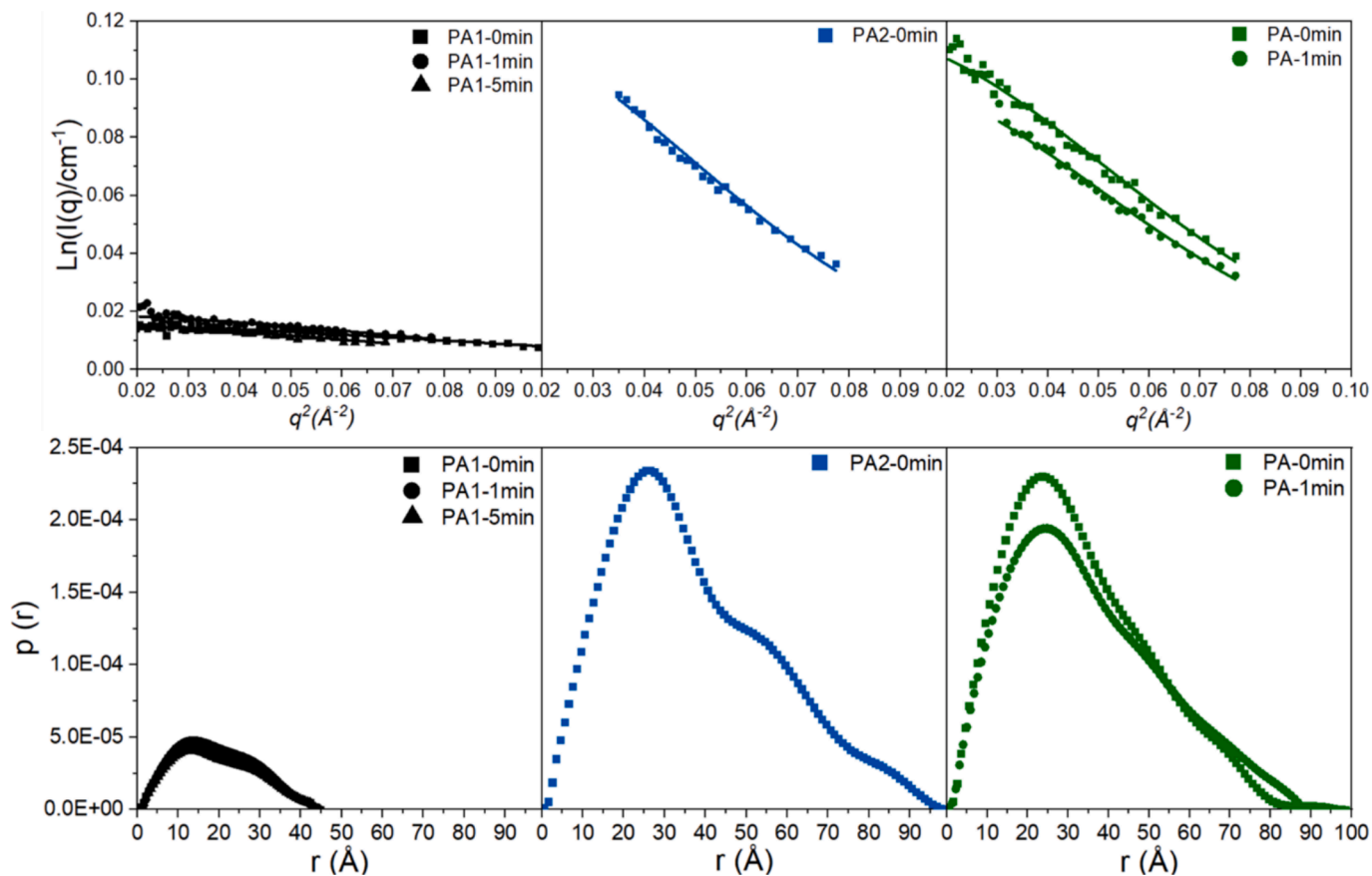


**Fig. 6.** Guinier plots (top) and distance distribution functions  $p(r)$  derived from Indirect Fourier Transformation (IFT) (bottom) calculated from the scattering intensities in the  $q$  range not disturbed by the power-law scattering at the high  $q$  range, for pea albumin solutions (10 mg/mL), namely PA1, PA2, and PA before (filled squares) and after heating at 90 °C for 1 min (filled circles), 5 min (filled triangles).

formation of increasingly compact aggregates. The formation of large aggregates in PA solutions explained the visual observations (Fig. 4).

### 3.4. Interfacial properties of pea albumins

To evaluate the relationship between the structural changes and interfacial properties, the unrefined PA, as well as PA1 and PA2 fractions, were also studied using drop tensiometry. Fig. 7 shows the decrease in the surface tension values as a function of time for the proteins before and after heating. The steep decrease in the first few minutes of analysis demonstrated the protein's tendency to readily diffuse and adsorb at the air/water interface. This initial adsorption of the proteins plays a critical role in determining the rate at which interfaces form in a foam generated by gas sparging. This adsorption rate of pea albumins has been reported to be similar to other proteins with well-known foaming properties, such as whey protein isolate or egg white isolate [3]. After about 10 min, a second, slower decrease in surface tension was noted, indicating the reorganization of the proteins at the interface, with a pseudo-equilibrium plateau value of surface tension at long time scales. The interfacial tension values reached at pseudo equilibrium were lower for PA than for the purified fractions in both heated and unheated solutions. It is important to note that due to the unrefined nature of the albumin fractions, other surface-active components may have also contributed to lowering the interfacial free energy. Regardless of the protein, heated samples showed lower values of interfacial tension compared to their unheated counterparts. This result is in agreement with previous research on pea albumins, suggesting that the lower interfacial tension relates to increased flexibility of the heat denatured albumins [39].

After the adsorption experiments, the loaded interfaces were subjected to dilatational experiments (Fig. 8). The various protein fractions showed dramatically different viscoelastic properties. The loss moduli ( $E_d''$ ) of all samples were in the range of 1–10 mN/m (data not shown), suggesting that the interfaces were more elastic than viscous in the applied regime. It was observed that plant albumins exhibited rheological behavior at the interface similar to that of whey protein isolate-stabilized films, forming stiff and cohesive layers capable of being compressed into a denser state [3].

PA1 displayed the highest surface tension and lower elastic modulus ( $E_d'$ ). This was probably due to PA1's small size [17], limiting protein's ability to spread at the interface. There were little differences in the rheological properties between the unheated and the heated PA1, in agreement with the structural studies (Figs. 4 and 5) showing little difference after extensive heating. The decreasing surface tension of heated PA1 solutions with increased heating time may indicate that the PA1 aggregates improved their adsorption properties, as shown by a decrease in interfacial tension, while keeping their original structure.

This resulted in no changes in their dilatational modulus,  $E_d'$ , across the entire deformation range.

In the case of PA2, the interfacial tension at pseudo equilibrium was higher for the native dimer, compared to the unfolded and aggregated proteins (Fig. 7). Furthermore, Fig. 8 revealed a higher dilatational modulus ( $E_d'$ ) and more amplitude-dependent for the unheated than heated PA2. When comparing PA2 with the whole PA solutions at the air/water interface (Figs. 7 and 8), it was suggested that the PA behavior was dominated by PA2, as similar viscoelastic properties were noted between the two preparations. However, the contribution of additional surface active molecules in PA could not be fully ruled out. The unheated PA2 solutions showed both higher surface tension and  $E_d'$ , and an amplitude-dependent behavior, indicating that these interfacial films were subject to increasing structural disruption with amplitude. This is consistent with a recent study reporting that PA2 exhibited high conformational rearrangement at the oil–water interface [37]. The stiffness and brittleness of the interface may be due to the presence of intramolecular disulfide bonds in the PA2 monomers. The lower overlapped  $E_d'$  for heated PA2 after 1 and 5 min heating indicated that the structures of the unfolded and more compact PA2 aggregates formed a less elastic network, but were more resistant to deformation. When comparing the dilatational modulus of PA to that of PA2 solutions, there were some differences, which cannot be fully explained due to the multiple factors that may have affected the interface. The network was more resilient in PA interfaces compared to PA2. With heating, PA water/air interfaces showed the stiffest dilatational modulus. It has been previously proposed that after heating the large colloidal PA aggregates dominate the oil–water interface [40]; however, multiple factors could contribute to the viscoelastic changes due to the unrefined nature of the preparation.

### 3.5. Foaming properties of pea albumins

The foaming properties of the albumins have also been found to be similar or better than whey protein and egg white isolate [3]. In this study, the foaming properties of the albumins and their fractions were investigated using the gas injection method, and the evolution of foam volume, liquid drainage, and bubble size variation were monitored. The results are shown in Fig. 9. Time zero was defined as the starting point of gas injection. After approximately 4 min, the gas injection was stopped, when a set foam volume (250 mL) was reached. Both unheated and heated samples of PA2 and PA reached the limit at almost the same time, and then they also evolved through a similar free drainage process for 90 min. PA1 solutions did not form foams under the same conditions, creating bubbles which collapsed immediately.

The foam height of the unheated PA2 was only slightly higher than that of the heated one, which was opposite to what was observed for the

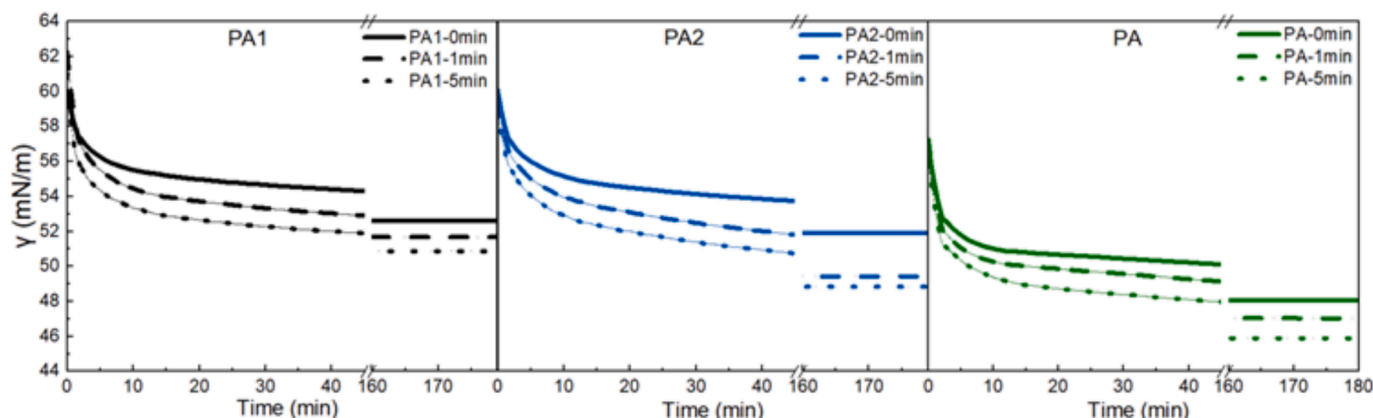


Fig. 7. Interfacial tension measured as a function of time for pea albumin solutions (1 mg/mL), namely, PA1, PA2, and PA before (solid line) or after heating at 90 °C for 1 min (broken line) or 5 min (dotted line). Measurements were in triplicate.

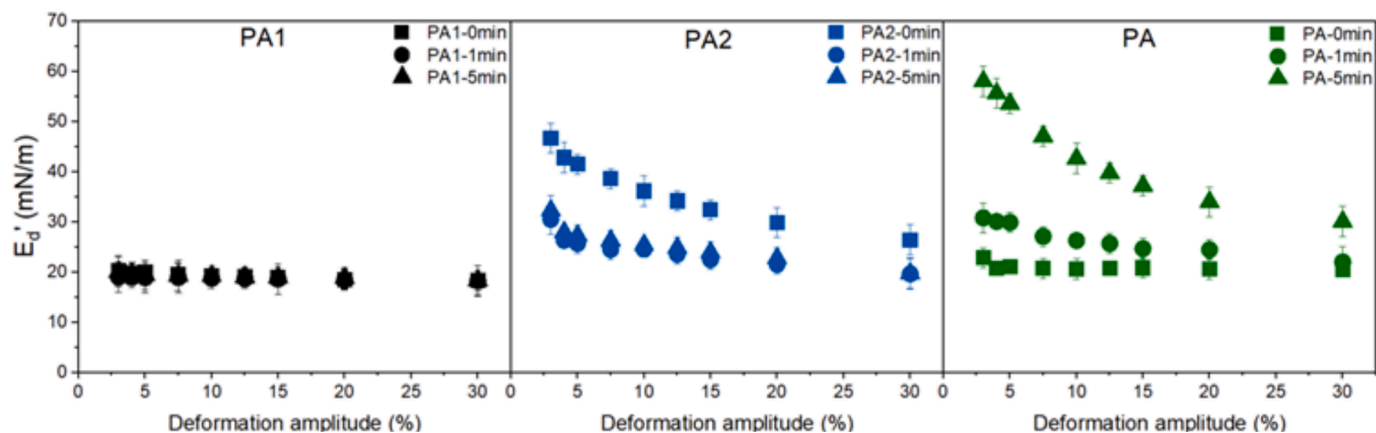


Fig. 8. The surface dilatational storage moduli ( $E_d'$ ) as a function of the amplitude of pea albumins covered interfaces, namely, PA1, PA2, and PA before (rectangular symbol) or after heating at 90 °C for 1 min (circle symbol) or 5 min (triangle symbol). Measurements were in triplicate.

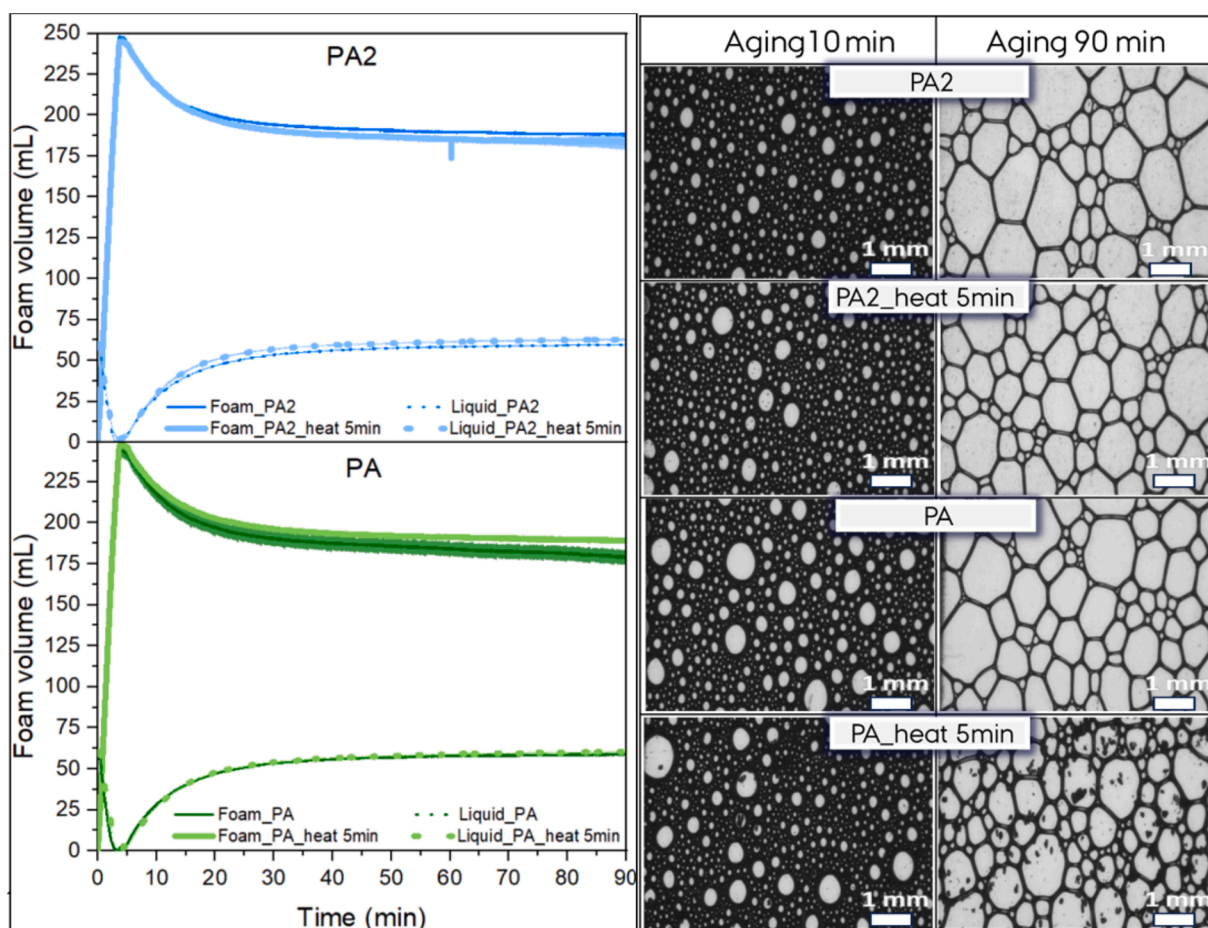


Fig. 9. Left: volume of foam (solid line) and solution (dashed line) as a function of time, for PA2 and PA solutions, thin line for unheated foam and thick line for heated 5 min foam. The standard deviations are plotted as the shaded region from three independent measurements. Right: Bubble shape and size at 10 and 90 min of aging. Results are representative of 3 independent experiments. PA1 are not shown as foams could not be formed. Measurements were in triplicate.

unfractionated albumin PA. However, the aggregates formed after heating seem not to affect their foam height in these measurements. As observed from Fig. 4, the sizes of PA aggregates were clearly larger than those from PA2. These insoluble aggregates in PA were expected to either reduce the effective concentration of proteins available for foaming or physically hinder the adsorption of soluble proteins to the interface, but they functioned the opposite. The bubbles became larger over time and changed in shape from spherical (wet foam) to polyhedral

(dry foam). In general, the samples did not show significant differences in their bubble sizes among the samples with aging time (results not shown). Furthermore, the effect of heat treatment did not contribute to significant differences of the foam stability for the pea albumins and their fraction, and the foam height of PA2 and PA were relatively stable over the aging time, indicating the albumins are promising as a foaming agent and PA2 is the dominating protein at the interface. When comparing these results to the viscoelastic properties measured by drop

tensiometry (Figs. 7 and 8), it may be suggested that in all cases, PA2 was adsorbing at the interface, and there was sufficient elasticity to form and maintain the bubble, slowing down the disproportionation, and higher resistance against coalescence. The PA2 albumin demonstrated higher foaming and emulsifying properties compared to the other low-MW hydrophilic and hydrophobic albumin fractions, likely due to the structure of the polypeptide chains [7].

#### 4. Conclusions

In this work, we investigated with an in-depth structural characterization, the contribution of PA1 and PA2 to the structure–function properties of pea albumins. It was hypothesized that the two proteins modify their structure once heated and that their contribution in a pea albumin isolate can be studied using a detailed structural analysis of PA1 and PA2 using SAXS based on high-resolution AlphaFold predictions. Our findings using FTIR spectroscopy indicated that PA2 fractions showed high  $\beta$ -sheet/ $\alpha$ -helix structures. From the modelling of the SAXS curves, PA1 remained folded upon heating and displayed limited aggregation. In contrast, PA2 existed as a dimer, and heating caused it to unfold and form large aggregates, resulting in a turbid solution. The detailed modeling of X-ray scattering intensities also demonstrated the different contributions of PA1 and PA2 in the heat-induced aggregation of the unfractured PA, suggesting a protective effect of PA1 or other minor components.

The structural changes described using SAXS were fundamental in understanding the impact of PA1 and PA2 in the interfacial and foaming properties of PA. While both PA1 and PA2 seem to adsorb at the interface and form elastic interfaces, PA2 contributes to the foaming properties of PA. PA2 forms stiffer interfaces resulting in stable foams, in contrast with PA1, which in isolation, forms bubbles with immediately collapse. After heating, aggregates are also able to form stable foam. Compared to the previous studies limited to the entire albumin extract [3,17], this study bridges the gap of establishing a detailed mechanistic understanding of the structure–function relationships of the individual protein components within the pea albumin mixture. These findings open new avenues to study the structural organization of complex food protein mixtures by establishing the relationship between the protein structure, aggregate states, and their interfacial and foaming properties, and give further insights into the utilization of promising food ingredients.

#### CRedit authorship contribution statement

**Ruifen Li:** Writing – review & editing, Writing – original draft, Visualization, Validation, Software, Methodology, Investigation, Formal analysis, Conceptualization. **Dionysios Neofytos:** Writing – review & editing, Validation, Methodology. **Jacob J.K. Kirkensgaard:** Writing – review & editing, Validation, Methodology. **Antara Pal:** Writing – review & editing, Validation. **Jan Skov Pedersen:** Writing – review & editing, Validation, Software, Methodology, Formal analysis, Conceptualization. **Milena Corredig:** Writing – review & editing, Validation, Supervision, Resources, Project administration, Investigation, Funding acquisition, Conceptualization.

#### Declaration of competing interest

The authors declare that they have no known competing financial interests or personal relationships that could have appeared to influence the work reported in this paper.

#### Acknowledgements

SAXS data was generated via a research infrastructure at the University of Copenhagen, partly funded by FOODHAY (Food and Health Open Innovation Laboratory, Danish Roadmap for Research

Infrastructure). This work was funded by Novo Nordisk Fund (NNF22OC0079708) - Post Doctoral Fellowship for research within plant science, agriculture and food biotechnology, the SupraPEA project under Plant2Food (Activity number 96804) funded by the Novo Nordisk Foundation, and the Villum Fonden (37759), through the Villum investigator award. Minh Tuan Tran and Hanne Søndergaard Møller were greatly appreciated for their help in SDS-PAGE and 2D gel electrophoresis methods.

#### Appendix A. Supplementary data

Supplementary data to this article can be found online at <https://doi.org/10.1016/j.jcis.2025.137507>.

#### Data availability

Data will be made available on request.

#### References

- [1] D. Chéreau, P. Videcoq, C. Ruffieux, L. Pichon, J.-C. Motte, S. Belaid, J. Ventureira, M. Lopez, Combination of existing and alternative technologies to promote oilseeds and pulses proteins in food applications, *OCL* 23 (4) (2016) D406.
- [2] A. Kimura, T. Fukuda, M. Zhang, S. Motoyama, N. Maruyama, S. Utsumi, Comparison of physicochemical properties of 7S and 11S globulins from Pea, Fava Bean, Cowpea, and french bean with those of soybean french bean 7S globulin exhibits excellent properties, *J. Agric. Food Chem.* 56 (21) (2008) 10273–10279.
- [3] J. Yang, R. Kornet, C.F. Diedericks, Q. Yang, C.C. Berton-Carabin, C.V. Nikiforidis, P. Venema, E. van der Linden, L.M.C. Sagis, Rethinking plant protein extraction: Albumin—From side stream to an excellent foaming ingredient, *Food Struct.* 31 (2022) 100254.
- [4] J. Yang, A. de Wit, C.F. Diedericks, P. Venema, E. van der Linden, L.M.C. Sagis, Foaming and emulsifying properties of extensively and mildly extracted Bambara groundnut proteins: a comparison of legumin, vicilin and albumin protein, *Food Hydrocoll.* 123 (2022) 107190.
- [5] S. Mundi, R.E. Aluko, Physicochemical and functional properties of kidney bean albumin and globulin protein fractions, *Food Res. Int.* 48 (1) (2012) 299–306.
- [6] S.A. Malomo, R.E. Aluko, A comparative study of the structural and functional properties of isolated hemp seed (*Cannabis sativa* L.) albumin and globulin fractions, *Food Hydrocoll.* 43 (2015) 743–752.
- [7] B.Y. Lu, L. Quillien, Y. Popineau, Foaming and emulsifying properties of pea albumin fractions and partial characterisation of surface-active components, *J. Sci. Food Agric.* 80 (13) (2000) 1964–1972.
- [8] R. Kornet, J. Yang, P. Venema, E. van der Linden, L.M.C. Sagis, Optimizing pea protein fractionation to yield protein fractions with a high foaming and emulsifying capacity, *Food Hydrocoll.* 126 (2022) 107456.
- [9] H.E. Schroeder, Quantitative studies on the cotyledonary proteins in the genus *Pisum*, *J. Sci. Food Agric.* 33 (7) (1982) 623–633.
- [10] T. Higgins, P. Chandler, P. Randall, D. Spencer, L. Beach, R. Blagrove, A. Kortt, A. Inglis, Gene structure, protein structure, and regulation of the synthesis of a sulfur-rich protein in pea seeds, *J. Biol. Chem.* 261 (24) (1986) 11124–11130.
- [11] T.J. Higgins, L.R. Beach, D. Spencer, P.M. Chandler, P.J. Randall, R.J. Blagrove, A. A. Kortt, R.E. Guthrie, cDNA and protein sequence of a major pea seed albumin (PA 2: Mr $\approx$  26 000), *Plant Mol. Biol.* 8 (1987) 37–45.
- [12] M. Varadi, D. Bertoni, P. Magana, U. Paramval, I. Pidruchna, M. Radhakrishnan, M. Tsenkov, S. Nair, M. Mirdita, J. Yeo, AlphaFold Protein Structure Database in 2024: providing structure coverage for over 214 million protein sequences, *Nucleic Acids Res.* 52 (D1) (2024) D368–D375.
- [13] P. Shewry, Plant storage proteins, *Biol. Rev. Camb. Philos. Soc.* (1995) 375–426.
- [14] L. Jouvansal, L. Quillien, E. Ferrasson, Y. Rahbé, J. Guéguen, F. Vovelle, PA1b, an insecticidal protein extracted from pea seeds (*Pisum sativum*):  $^1\text{H}$ -2-D NMR study and molecular modeling, *Biochemistry* 42 (41) (2003) 11915–11923.
- [15] L. Karaki, P. Da Silva, F. Rizk, C. Chouabe, N. Chantret, V. Eyraud, F. Gressent, C. Sivignon, I. Rahioui, D. Kahn, Genome-wide analysis identifies gain and loss/change of function within the small multigenic insecticidal Albumin 1 family of *Medicago truncatula*, *BMC Plant Biol.* 16 (1) (2016) 1–19.
- [16] R.R. Croy, M.S. Hoque, J.A. Gatehouse, D. Boulter, The major albumin proteins from pea (*Pisum sativum* L). Purification and some properties, *Biochem. J.* 218 (3) (1984) 795–803.
- [17] R. Li, J.J. Kirkensgaard, M. Corredig, Structural evolution of pea-derived albumins during pH and heat treatment studied with light and X-ray scattering, *Food Res. Int.* 186 (2024) 114380.
- [18] S.S. Nielsen, Phenol-sulfuric acid method for total carbohydrates, *Food Anal. Lab. Manual.* (2010) 47–53.
- [19] L.B. Larsen, A. Wedholm-Pallas, H. Lindmark-Månsson, A. Andrén, Different proteomic profiles of sweet whey and rennet casein obtained after preparation from raw versus heat-treated skimmed milk, *Dairy Sci. Technol.* 90 (6) (2010) 641–656.

- [20] M. Jackson, H.H. Mantsch, The use and misuse of FTIR spectroscopy in the determination of protein structure, *Crit. Rev. Biochem. Mol. Biol.* 30 (2) (1995) 95–120.
- [21] E. Goormaghtigh, V. Cabiaux, J.M. Ruysschaert, Secondary structure and dosage of soluble and membrane proteins by attenuated total reflection Fourier-transform infrared spectroscopy on hydrated films, *Eur. J. Biochem.* 193 (2) (1990) 409–420.
- [22] D.D. Neofytos, A. Papagiannopoulos, E.D. Chrysina, S. Pispas, Formation and physicochemical properties of glycogen phosphorylase in complex with a cationic polyelectrolyte, *Int. J. Biol. Macromol.* 206 (2022) 371–380.
- [23] M. Toplak, S.T. Read, C. Sandt, F. Borondics, Quasar: easy machine learning for biospectroscopy, *Cells* 10 (9) (2021) 2300.
- [24] M. Toplak, G. Birarda, S. Read, C. Sandt, S. Rosendahl, L. Vaccari, J. Demšar, F. Borondics, Infrared orange: connecting hyperspectral data with machine learning, *Synchrotron Radiat. News.* 30 (4) (2017) 40–45.
- [25] M. Wojdyr, Fityk: a general-purpose peak fitting program, *J. Appl. Crystallogr.* 43 (5) (2010) 1126–1128.
- [26] V. Iconomidou, D. Chryssikos, V. Gionis, M. Pavlidis, A. Paipetis, S. Hamdrakas, Secondary structure of chorion proteins of the teleostean fish *Dentex dentex* by ATR FT-IR and FT-Raman spectroscopy, *J. Struct. Biol.* 132 (2) (2000) 112–122.
- [27] A. Mauerer, G. Lee, Changes in the amide I FT-IR bands of poly-L-lysine on spray-drying from  $\alpha$ -helix,  $\beta$ -sheet or random coil conformations, *Eur. J. Pharm. Biopharm.* 62 (2) (2006) 131–142.
- [28] J. de la Rosa-Millán, J.L. Orona-Padilla, V.M. Flores-Moreno, S.O. Serna-Saldívar, Physicochemical, functional and ATR-FTIR molecular analysis of protein extracts derived from starchy pulses, *Int. J. Food Sci. Technol.* 53 (6) (2018) 1414–1424.
- [29] E.M. Steiner, J. Lyngsø, J.E. Guy, G. Bourenkov, Y. Lindqvist, T.R. Schneider, J. S. Pedersen, G. Schneider, R. Schnell, The structure of the N-terminal module of the cell wall hydrolase RipA and its role in regulating catalytic activity, *Proteins: Struct. Funct. Bioinform.* 86 (9) (2018) 912–923.
- [30] R.L. Bærentsen, S.V. Nielsen, R.B. Skjerning, J. Lyngsø, F. Bisiak, J.S. Pedersen, K. Gerdes, M.A. Sørensen, D.E. Brodersen, Structural basis for kinase inhibition in the tripartite *E. coli* HipBST toxin–antitoxin system, *Elife* 12 (2023) RP90400.
- [31] K.M. Coulter, J.D. Bewley, Characterization of a small sulphur-rich storage albumin in seeds of alfalfa (*Medicago sativa* L.), *J. Exp. Bot.* 41 (12) (1990) 1541–1547.
- [32] L.C. Gruen, R.E. Guthrie, R.J. Blagrove, Structure of a major pea seed albumin: implication of a free sulphhydryl group, *J. Sci. Food Agric.* 41 (2) (1987) 167–178.
- [33] M.A. Soliman, A. Khedr, M.A. Elsayy, Peptide and protein emulsifiers, in: M. A. Elsayy (Ed.), *Peptide Bionanomaterials: from Design to Application*, Springer, Cham, 2023, pp. 431–474.
- [34] W. Norde, The behaviour of proteins at interfaces in relation to their structural stability, *Stud. Org. Chem. Elsevier* (1993) 3–11.
- [35] K. Abrosimova, O. Shulenina, S. Paston, FTIR study of secondary structure of bovine serum albumin and ovalbumin, *J. Phys. : Conference Series* 769 (1) (2016) 012016.
- [36] S. Le Maux, S. Bouhallab, L. Giblin, A. Brodkorb, T. Croguennec, Bovine  $\beta$ -lactoglobulin/fatty acid complexes: binding, structural, and biological properties, *Dairy Sci. Technol.* 94 (2014) 409–426.
- [37] Y. Luo, W. Zheng, Q. Shen, L. Zhang, C. Tang, R. Song, S. Liu, B. Li, Y. Chen, Adsorption kinetics and dilatational rheological properties of recombinant Pea Albumin-2 at the oil-water interface, *Food Hydrocoll.* 120 (2021) 106866.
- [38] L. Schrodinger, *The PyMOL molecular graphics system, Version 1* (2015) 8.
- [39] Y. Djemaoune, E. Cases, R. Saurel, The effect of high-pressure microfluidization treatment on the foaming properties of pea albumin aggregates, *J. Food Sci.* 84 (8) (2019) 2242–2249.
- [40] K.F. Grasberger, F.W. Lund, A.C. Simonsen, M. Hammershøj, P. Fischer, M. Corredig, Role of the pea protein aggregation state on their interfacial properties, *J. Colloid Interface Sci.* 658 (2024) 156–166.